

An atomistic study of defect energetics and diffusion with respect to composition and temperature in γ U and γ U-Mo alloys

Gyuchul Park^a, Benjamin Beeler^{b,c}, Maria A. Okuniewski^{a,*}

^aSchool of Materials Engineering, Purdue University, West Lafayette, IN 47907, United States

^bDepartment of Nuclear Engineering, North Carolina State University, Raleigh, NC 27695, United States

^cIdaho National Laboratory, Idaho Falls, ID 83415, United States

Abstract

Uranium-molybdenum (U-Mo) alloys are promising candidates for high-performance research and test reactors, as well as fast reactors. The metastable γ phase, which shows acceptable irradiation performance, is retained by alloying U with Mo with specific quenching conditions. Point defects contribute to the atomic diffusion process, defect clustering, creep, irradiation hardening, and swelling of nuclear fuels, all of which play a role in fuel performance. In this work, properties of point defects in γ U and γ U-xMo ($x = 7, 10, 12$ wt.%) were investigated. Vacancy and self-interstitial formation energies in γ U and γ U-xMo were calculated with molecular dynamics (MD) simulations using an embedded atom method interatomic potential for the U-Mo system. Formation energies of point defects were calculated in the temperature range between 400 K and 1200 K. The vacancy formation energy was higher than the self-interstitial formation energy in both γ U and γ U-xMo in the evaluated temperature range, which supports the previous results obtained via first-principles calculations and MD simulations. In γ U-xMo, the vacancy formation energy decreased with increasing Mo content, whereas the self-interstitial formation energy increased with increasing Mo content in the temperature range of 400 K to 1200 K. The self-diffusion and interdiffusion coefficients were also determined in γ U-xMo as a function of temperature. Diffusion of U and Mo atoms in γ U-xMo were negligible below 800 K. The self-diffusion and interdiffusion coeffi-

*Corresponding author. Purdue University, West Lafayette, IN 47907, USA
Email address: mokuniew@purdue.edu (Maria A. Okuniewski)

ients decreased with increasing Mo concentration, which qualitatively agreed with the previous experimental observations. Point defect formation energies, self-diffusion coefficients, and interdiffusion coefficients in γ U-xMo calculated in the present work can be used as input parameters in **microscale and mesoscale** fuel performance modeling.

Keywords: uranium, uranium-molybdenum (U-Mo) alloys, defect energetics, diffusion, self-diffusion coefficients, interdiffusion coefficients, molecular dynamics

1. Introduction

Uranium-molybdenum (U-Mo) alloys are considered as one possible candidate for nuclear fuels for future fast reactors, as well as high-performance research and test reactors (HPRRs) [1, 2, 3]. For example, HPRRs such as the Advanced Test Reactor at Idaho National Laboratory and the High-Flux Isotope Reactor at Oak Ridge National Laboratory, require a higher uranium density (> 6.5 g/cc) due to flux requirements, as compared to other research reactors. Pure uranium contains three allotropes according to the phase diagram: α U (orthorhombic crystal structure, below 668°C), β U (tetragonal crystal structure, between 668°C and 776°C), and γ U (body-centered cubic crystal structure (bcc), between 776°C and 1135°C) [4]. During reactor operation, pure α U fuel exhibits anisotropic growth and anisotropic swelling under irradiation, which has historically limited the usage of unalloyed α U [5, 6]. On the other hand, γ U exhibits isotropic swelling behavior, therefore displays comparatively better irradiation performance than α U [6, 7]. Thus, metastable γ U, obtained by alloying Mo with U followed by rapid cooling, has been utilized as nuclear fuel. U-Mo alloys containing less than 6 wt.% Mo yield a high fraction of undesirable decomposed phases (α U and γ' U); therefore, U-Mo alloys with a concentration of 7–12 wt.% Mo are of primary interest since the γ U phase is stabilized [8, 9, 10, 11].

Point defects exist in metals and alloys at thermal equilibrium, but they are also produced in great quantities under irradiation during nuclear reactor operations. Point defects are critical to fuel behavior since they play a key role in the atomic diffusion process, which affect the nucleation of extended defects, such as dislocations, dislocation loops, voids, and fission gas bubbles. Thus, point defects can affect the

macroscopic properties of the nuclear fuel, including creep, irradiation hardening, and swelling [12, 13, 14]. Additionally, point defects and their diffusion are critical parametric inputs into microscale and mesoscale simulations. Therefore, the incorporation of accurate defect energetics and self-diffusion coefficients will increase the fidelity of these modeling codes.

The formation energy of point defects in γ U has been determined via both experimental and computational simulation techniques. The historical results obtained via positron annihilation spectroscopy (PAS) and *ab initio* methods are represented in Table 1. The authors are not aware of any experimental data that exists for self-interstitial formation energy in γ U. Vacancy formation energy, experimentally calculated by PAS, ranged between 0.3 eV and 1.6 eV [15, 16, 17, 18, 19]. Lund et al. [18, 19] attributed the variation in experimentally determined vacancy formation energies to differing specimen geometries, which contained varying oxygen (O) impurity concentrations. This was further supported by first-principles calculations in α U, which showed that O defects reduced vacancy formation energies [19]. The vacancy formation energy of α U was calculated via first-principles calculations when an O atom was incorporated near a vacancy as a substitutional and an interstitial, respectively. A decrease in the vacancy formation energy of α U was proved irrespective of the position of O atom [19]. It should be noted that the vacancy formation energy calculated by Lund et al. (1.6 ± 0.2 eV) is the average value over the temperature range from 300 K to 1200 K, indicating that the calculated vacancy formation energy is an average value of the α , β , and γ U phases [18, 19]. On the other hand, the vacancy formation energy in γ U calculated by *ab initio* methods ranged between 1.08 eV and 1.38 eV [20, 21] using the Perdew-Wang 91 (PW 91) and the Perdew-Burke-Ernzerhof (PBE) generalized gradient approximation functionals [22, 23]. The discrepancy of 0.3 eV can be attributed to the use of different exchange-correlation functionals, as well as different methodologies.

The self-interstitial formation energy, calculated via *ab initio* methods, was found to be strongly contingent on the configuration of the self-interstitial [21]. The <100> dumbbell and tetrahedral sites were found to be the most and least stable configurations, respectively [21]. In addition, an anomalously high self-diffusion coefficient was observed in γ U when compared to other bcc metals, which can be attributed to the

55 dominance of self-interstitials in the diffusion process [24, 25, 26, 27].
 56 In γ U-Mo, there is a lack of data for point defect energetics. To the best of the
 57 authors' knowledge, experimental data does not exist, and the only investigations of
 58 point defects energetics in γ U-Mo utilizes molecular dynamics (MD) studies in γ U-
 59 Mo at 1000 K [26] and γ U-10Mo at 400 K [28] at zero pressure. This lack of data has
 60 motivated the current study investigating the defect energetics of both γ U and γ U-Mo
 61 as a function of temperature and composition using MD simulations. Using the point
 62 defect energetics, the self-diffusion coefficients in γ U-xMo ($x = 7, 10, 12$ wt.%) are
 63 also calculated with respect to temperature, and compared to experimental results.

Table 1: Vacancy (E_{vac}^f) and self-interstitial (E_{self-i}^f) formation energies in γ U, obtained by PAS and *ab initio* methods.

Method	E_{vac}^f (eV)	E_{self-i}^f (eV)	References
PAS	1.17	—	[15]
	1.2 ± 0.25	—	[16]
	0.3	—	[17]
	1.6 ± 0.2	—	[18, 19]
<i>ab initio</i>	1.08 (PW91)	—	[20]
	1.32 (PW91), 1.38 (PBE)	0.50–1.54	[21]

64 2. Computational Details

65 MD simulations were conducted to calculate defect formation energies in γ U and
 66 γ U-xMo as a function of temperature, as well as the self-diffusion coefficients in γ U-
 67 xMo, using the LAMMPS software package [29]. The accuracy of MD simulations
 68 greatly depends on the accuracy of the interatomic potential used. Embedded atom
 69 method (EAM) interatomic potentials have been used extensively in the study of defect
 70 properties in metals and alloys [30, 31, 32, 33, 34, 35]. The success of EAM potentials
 71 to describe metallic systems is derived from its formalism in describing many body
 72 interactions, which pair-wise potentials are unable to do.

73 A general form of the EAM potential is described as follows [30, 36]:

$$E_{total} = \frac{1}{2} \sum_{i < j} \phi_{ij}(r_{ij}) + \sum_i F(\sum_{j \neq i} \rho_i(r_{ij})), \quad (1)$$

74 where E_{total} is the total energy of the system, ϕ_{ij} is the pair-wise energy term, which de-
75 pends on the distance (r_{ij}) between two given atoms i and j . The term $F(\sum_{j \neq i} \rho_i(r_{ij}))$
76 is the embedding energy of atom i , which defines the many-body interatomic interac-
77 tions, depending on the background electron density (ρ_i) at the location of atom i . The
78 total energy from the pair-wise energy term is divided by two to avoid double count-
79 ing. In this study, the EAM potential for the ternary U-Mo-Xe system, developed by
80 Smirnova et al. [37], was utilized. This potential was selected since it has successfully
81 reproduced characteristic material properties, such as lattice parameter, Young's modu-
82 lus, room-temperature density and melting temperature of U-10Mo alloys [37]. More-
83 over, this potential is the only interatomic potential capable of describing the ternary U-
84 Mo-Xe system. This work complements recent atomistic investigations on fundamental
85 void and Xe bubble properties in γ U and γ U-Mo systems [21, 28, 38, 39, 40, 41, 42].

86 A $10 \times 10 \times 10$ simulation cell (2,000 atoms) of γ U was created with periodic bound-
87 ary conditions. A large system was utilized to approximate the random substitutional
88 solid solution alloys and thus avoided the interaction of the point defects with periodic
89 boundary conditions. For the alloy systems, a fraction of U atoms were changed to Mo
90 atoms, corresponding to a given weight percent (7, 10, and 12 wt.%) to reflect typical
91 fuel alloy concentrations. The U atoms were replaced with Mo atoms at randomly dis-
92 tributed lattice sites, generating a solid substitutional alloy. The system was relaxed for
93 200 ps with a timestep of 0.002 ps in an NPT ensemble with a Langevin thermostat in
94 the Gronbech-Jenson-Farago formalism [43, 44]. The evaluated temperatures ranged
95 between 400 K and 1200 K in increments of 200 K at zero pressure. The low and high
96 temperature ranges correspond to the operating temperatures for research reactors and
97 fast reactors, respectively. The γ U phase was the only phase observed in the evaluated
98 temperatures using the Adaptive Common Neighbor Analysis in the OVITO software
99 [45, 46, 47]. Once the system reached equilibrium, a point defect (a vacancy or a self-
100 interstitial) was created. Equilibrium of the system was confirmed by investigating the
101 potential energy of the system as a function of time. The potential energy stayed nearly

102 constant after 10 ps, indicating that the system reached equilibrium at this time. The
 103 Wigner-Seitz defect analysis in the OVITO software was used to ensure that only a
 104 single point defect (vacancy or self-interstitial) was created during the simulations. It
 105 is noteworthy that both U and Mo atoms were separately removed from the system to
 106 calculate the vacancy formation energy, and added to the system to calculate the self-
 107 interstitial formation energy. Thus, this study does not represent the defect properties
 108 of a single element in the alloy, but rather the average defect properties of the alloy.
 109 One hundred unique simulations were conducted in γ U at each temperature. More than
 110 400 unique simulations in γ U-xMo, with random Mo positions at each temperature and
 111 composition were performed to ensure the statistical significance of the dataset.

112 Vacancy ($E_{vac,\gamma U}^f$) and self-interstitial ($E_{self-i,\gamma U}^f$) formation energies in γ U were
 113 calculated as described below:

114

$$E_{vac,\gamma U}^f = E_{vac} - \frac{(N-1)}{N} E_{ideal}, \quad (2)$$

115

116 where N is the number of atoms in the system without defects, E_{ideal} is the potential en-
 117 ergy of the system without defects, E_{vac} is the potential energy of the system containing
 118 a vacancy, and E_{self-i} is the potential energy of the system containing a self-interstitial.
 119 In addition, vacancy ($E_{vac,\gamma U-Mo}^f$) and self-interstitial ($E_{self-i,\gamma U-Mo}^f$) formation ener-
 120 gies in γ U-xMo were calculated as described below:

121

$$E_{vac,\gamma U-Mo}^f = E_{FE(vac)} - \frac{(N-1)}{N} E_{FE(ideal)}, \quad (4)$$

$$E_{self-i,\gamma U-Mo}^f = E_{FE(self-i)} - \frac{(N+1)}{N} E_{FE(ideal)}, \quad (5)$$

122 where $E_{FE(ideal)}$ is the formation energy of the system without defects, $E_{FE(vac)}$ is the
 123 formation energy of the system containing a vacancy, and $E_{FE(self-i)}$ is the formation
 124 energy of the system containing a self-interstitial. The formation energy of the system

¹²⁵ without defects was calculated as follows:

$$E_{FE(ideal)} = E_{ideal} - (E_U N_U + E_{Mo} N_{Mo}) \quad (6)$$

¹²⁶ where N_U is the number of U atoms, N_{Mo} is the number of Mo atoms, E_U is the potential
¹²⁷ energy per atom in γ U, and E_{Mo} is the potential energy per atom in Mo. Note that the
¹²⁸ crystal structure of Mo is also bcc. In the same way, the formation energies of the
¹²⁹ system containing a vacancy and a self-interstitial were calculated as follows:

$$E_{FE(vac)} = E_{vac} - (E_U N_U + E_{Mo} N_{Mo}) \quad (7)$$

¹³⁰

$$E_{FE(self-i)} = E_{self-i} - (E_U N_U + E_{Mo} N_{Mo}) \quad (8)$$

¹³¹ It should be noted that, in the case of γ U where $N_{Mo}=0$, Eq. (4) and (5) are simplified
¹³² into Eq. (2) and (3), respectively. The energies (E_{ideal} , E_{vac} , E_{self-i} , E_U , and E_{Mo}),
¹³³ calculated at each timestep, were averaged over the last 100 ps. Since a vacancy and a
¹³⁴ self-interstitial diffuse in the system during the simulation, the calculated vacancy and
¹³⁵ self-interstitial formation energy is an average over various defect configurations.

¹³⁶ Self-diffusion coefficients of U (D_{self-D}^U) and Mo atoms (D_{self-D}^{Mo}) in γ U-Mo were
¹³⁷ calculated using the following equations:

$$D_{self-D}^U = c_{vac} D_{vac}^U + c_{self-i} D_{self-i}^U, \quad (9)$$

¹³⁸

$$D_{self-D}^{Mo} = c_{vac} D_{vac}^{Mo} + c_{self-i} D_{self-i}^{Mo}, \quad (10)$$

¹³⁹ where D_{vac}^U is the diffusivity of U atoms in γ U-Mo containing a vacancy, D_{vac}^{Mo} is the
¹⁴⁰ diffusivity of Mo atoms in γ U-Mo containing a vacancy, D_{self-i}^U is the diffusivity of U
¹⁴¹ atoms in γ U-Mo containing a self-interstitial, D_{self-i}^{Mo} the diffusivity of Mo atoms in γ U-
¹⁴² Mo containing a self-interstitial, c_{vac} is the concentration of vacancies at equilibrium,
¹⁴³ and c_{self-i} is the concentration of self-interstitials at equilibrium. c_{vac} and c_{self-i} are
¹⁴⁴ expressed as follows:

$$c_{vac} = \exp\left(\frac{\Delta S_{vac}^f}{k_B}\right) \exp\left(\frac{-E_{vac}^f}{k_B T}\right) \quad (11)$$

$$c_{self-i} = \exp\left(\frac{\Delta S_{self-i}^f}{k_B}\right) \exp\left(\frac{-E_{self-i}^f}{k_B T}\right) \quad (12)$$

where $\Delta S_{vac/self-i}^f$ is the change in entropy by creating a vacancy or self-interstitial, k_B is the Boltzmann constant, and T is the temperature in Kelvin. In this work, similar to Smirnova et al. [27], it is assumed that the entropy does not affect the concentration of the point defects. $D_{vac}^{U/Mo}$ and $D_{self-i}^{U/Mo}$ can be obtained by the following equation:

$$D_{vac/self-i}^{U/Mo} = \frac{\sum_{i=1}^N \Delta r_i^2}{6t} \quad (13)$$

where Δr_i^2 is the mean-square displacement of the i th atom, and t is the simulation time. Once the system reached equilibrium, the mean-square displacements of both U and Mo atoms were obtained over 100 ns. Twenty unique simulations were conducted at each composition and temperature. Following this, the mean-square displacements were averaged. The interdiffusion coefficients ($D_{inter-D}^{U-xMo}$) in γ U-xMo were calculated using the self-diffusion coefficients with the Darken equation [48] to compare with experimental results:

$$D_{inter-D}^{U-xMo} = X_U D_{self-D}^{Mo} + X_{Mo} D_{self-D}^U \quad (14)$$

where X_U and X_{Mo} are the atomic fractions of U and Mo atoms in the alloy, respectively.

3. Results

3.1. Convergence tests

Numerous simulations were carried out to obtain the converged average potential energy of the systems for defect formation energy calculations. The convergence of the potential energy was verified by calculating the cumulative moving average of the potential energy as a function of the number of simulations. Fig. 1 represents the cumulative moving average of potential energies and the standard errors of the system without defects, with a vacancy, and with a self-interstitial in γ U at 1200 K with respect to the number of simulations, as an example. The cumulative moving averages of

167 the potential energy plateaued after approximately 50-60 simulations, which illustrated
 168 convergence. Another set of 100 simulations for the system without defects was con-
 169 ducted in γ U at 1200 K. The variance from 100 simulations and 200 simulations was
 170 only 0.05 eV, which further illustrated the convergence of the potential energy. The
 171 potential energy was different in each simulation (e.g. Fig. 1(a)), caused by random
 172 number seeds resulting in a different distribution of initial atom velocities. However,
 173 the variance was very small, as indicated by the standard errors in γ U without defects,
 174 with a vacancy, and with a self-interstitial, shown in Fig. 1(b). The standard errors of
 175 the three systems mentioned above continued to decrease as a function of the number
 176 of simulations. Therefore, it was determined that 100 independent simulations were
 177 sufficient to obtain converged potential energies in γ U for all three systems.

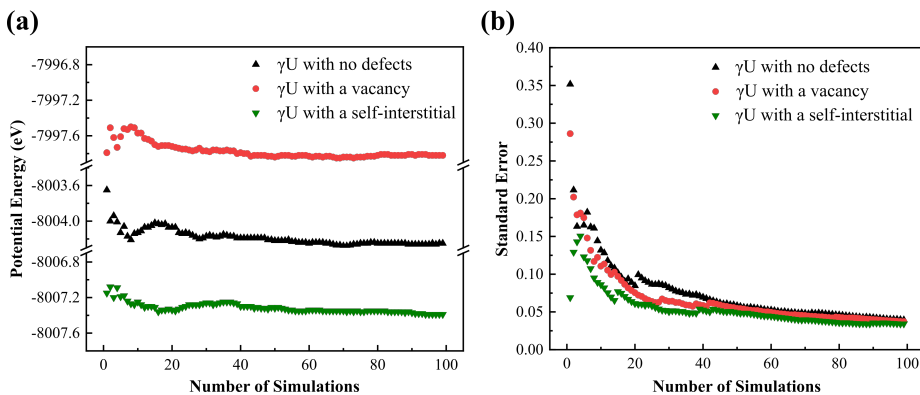


Figure 1: (a) The cumulative moving average of the potential energy at 1200 K in γ U without defects, with a vacancy, and with a self-interstitial. Note the discontinuities in the y axis used for visualization purposes.
 (b) Standard errors for the cumulative moving average of the potential energy in γ U without defects, with a vacancy, and with a self-interstitial. The standard error is defined as the standard deviations divided by the square root of the number of simulations.

178 A similar convergence procedure was carried out for γ U-xMo. The cumulative
 179 moving average of the potential energy and the standard error in γ U-12Mo at 1200 K
 180 are shown as a function of the number of simulations in Fig. 2, as an example. The con-
 181 centration of Mo in γ U-xMo was slightly different in each simulation. A given fraction
 182 of U atoms, x wt.% within the range of ± 1 wt.%, was changed to Mo atoms in each
 183 simulation. Following the completion of all simulations, the overall averages of the Mo

184 concentrations were 7, 10, and 12 wt.%. In the alloy systems, the cumulative moving
 185 averages of the potential energy were consistent after approximately 500 simulations,
 186 which demonstrated the convergence of the potential energy. The difference between
 187 the overall average potential energy from 500 simulations ~~and from~~ 1,000 simulations
 188 was very slight (0.10 eV), which further demonstrated the convergence of the potential
 189 energy. Due to the variation of potential energy in γ U-xMo, mostly resulting from the
 190 variability in the Mo concentration, a greater number of simulations was required to
 191 reach acceptable levels of error, and to obtain the converged potential energies.

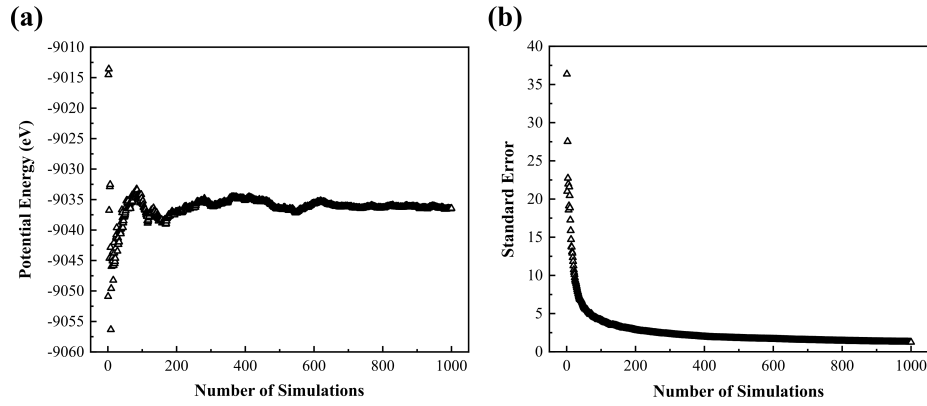


Figure 2: (a) The cumulative moving average of the potential energy in γ U-12Mo without defects at 1200 K. (b) Standard errors for the cumulative moving average of the potential energy in γ U-12Mo without defects. The standard error is defined by the standard deviations divided by the square root of the number of simulations.

192 3.2. Defect energetics in γ U

193 The historical results of vacancy and self-interstitial formation energies in γ U, cal-
 194 culated using MD simulations [27, 37, 49, 50] are shown in Fig. 3 along with the
 195 present work. Standard errors were calculated by summing the standard error of poten-
 196 tial energy of the perfect system and the standard error of potential energy of the system
 197 containing a vacancy/self-interstitial. The vacancy formation energies, determined us-
 198 ing the EAM U-Mo-Xe potential calculated at 500 K by Smirnova et al. [37] and at
 199 600 K in the current work, were nearly equivalent at 2.2 eV. In this work, the vacancy
 200 formation energy increased from 1.74 eV to 2.43 eV as the temperature increased from
 201 400 K to 1200 K, respectively. The vacancy formation energies, calculated with the

202 EAM U-Mo-Xe potential in this work, were greater than those from the modified EAM
203 (MEAM) U potential [49] from 800 K to 1200 K, but the trends were in qualitative
204 agreement, increasing with temperature. An increase in vacancy formation energy as a
205 function of temperature was also observed in other pure metals, such as Al, Fe, and Zr
206 [51, 52, 53]. The vacancy formation energies in γ U at 1000 K, calculated by Smirnova
207 et al. [50] and Beeler et al. [49] with the MEAM potential, were consistent with one
208 another. On the other hand, the vacancy formation energy at 1000 K calculated with
209 the EAM U potential [50] was 2.5 eV, higher than the vacancy formation energies, cal-
210 culated with the MEAM U and EAM U-Mo-Xe potentials.

211 The self-interstitial formation energy in γ U, calculated by Smirnova et al. [50] with
212 the MEAM U potential, was greater than that calculated by Beeler et al. [49] with the
213 same potential. However, both historical results indicated that the self-interstitial for-
214 mation energy increased as the temperature increased. On the other hand, this work
215 shows that there was little temperature dependency on the self-interstitial formation
216 energy in the evaluated temperature range. The lower and upper limits of the self-
217 interstitial formation energy were 0.90 eV and 1.08 eV, respectively. These results
218 agree with the self-interstitial formation energy calculated by Smirnova et al. [37]
219 with the identical potential in γ U. The self-interstitial formation energy in γ U was
220 approximately 1.05 eV, independent of the temperature [37]. The self-interstitial for-
221 mation energy, calculated by Smirnova et al. [27] with the EAM U potential, was
222 also temperature-independent in the range between 800 K and 1200 K. Both the va-
223 cancy and self-interstitial formation energies, obtained with the MEAM U potential,
224 decreased at 1300 K due to the spontaneous formation of Frenkel pairs in close prox-
225 imity to the melting point (approximately 1400 K) [49]. The vacancy formation energy
226 was greater than the self-interstitial formation energy at temperatures ranging from 400
227 K and 1200 K in γ U. This is notable since creating a self-interstitial requires additional
228 energy as compared to creating a vacancy in most metals [54, 55, 56, 57, 58]. How-
229 ever, these results agree with previous density functional theory work [21]. Although
230 different interatomic potentials produce varying results for vacancy and self-interstitial
231 formation energies in γ U, the current work compares well with previously published
232 results [27, 37, 49, 50]. Since each interatomic potential has different parameters that

233 are more or less accurate compared to the experimental data and the different range of
 234 applicability, the entire scope of data for different potentials was included.

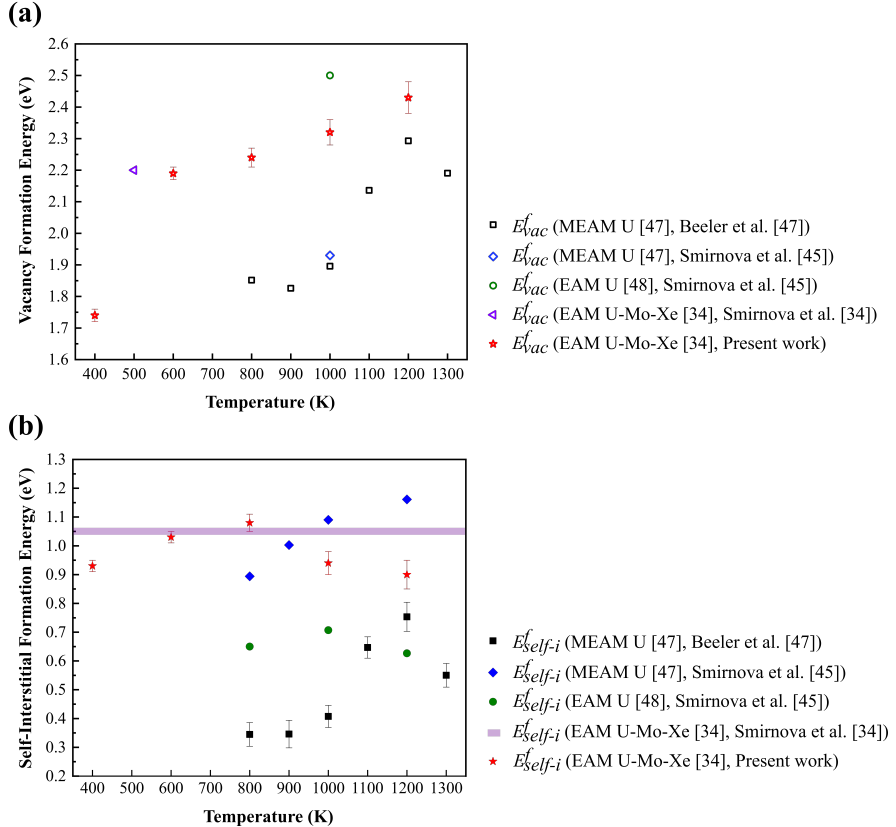


Figure 3: (a) Vacancy formation energy and (b) self-interstitial formation energy in γ U with respect to the temperature, comparing previous work using different interatomic potentials and the current work [27, 37, 49, 50]. Error bars indicated are standard errors.

235 3.3. Defect energetics in γ U-Mo

236 Fig. 4 shows the results of the vacancy and self-interstitial formation energy calcu-
 237 lations in γ U-xMo as a function of temperature. A strong temperature dependence was
 238 not evident for the vacancy formation energy. On the other hand, the self-interstitial
 239 formation energy tended to increase at temperatures greater than or equal to 600 K. The
 240 vacancy formation energy decreased with increasing Mo content in γ U-xMo for equiva-
 241 lent temperatures ranging from 400 K to 1200 K. Whereas, the self-interstitial formation

242 energy increased with increasing Mo content in γ U-xMo in the equivalent temperature
 243 range. Consequently, the difference between the vacancy and self-interstitial formation
 244 energy decreased with increasing Mo concentration at equivalent temperatures. As in
 245 γ U, the vacancy formation energy for each alloy was higher than the self-interstitial
 246 formation energy at the equivalent temperatures. These results qualitatively agree with
 247 the previous MD point defect studies in γ U-Mo [26, 28]. For example, the vacancy
 248 and self-interstitial formation energies calculated with the U-Mo-Xe potential were 1.4
 249 eV and 0.3 eV, respectively, in γ U-9Mo at 1000 K [26]. Using the same interatomic
 250 potential, the vacancy and self-interstitial formation energies were 1.6 eV and 1.1 eV,
 251 respectively, in γ U-10Mo at 400 K [28]. A discrepancy in the self-interstitial formation
 252 energy between the present work and Beeler's work [28] could originate from the dif-
 253 ferent methodology.ⁿ In Beeler's work [28], the number of simulations that a U atom
 254 was introduced was proportional to the concentration of U atoms in γ U-xMo. On the
 255 other hand, in the present work, the number of simulations that a U atom was introduced
 256 as the defect was the same as the number of simulations that a Mo atom was introduced.

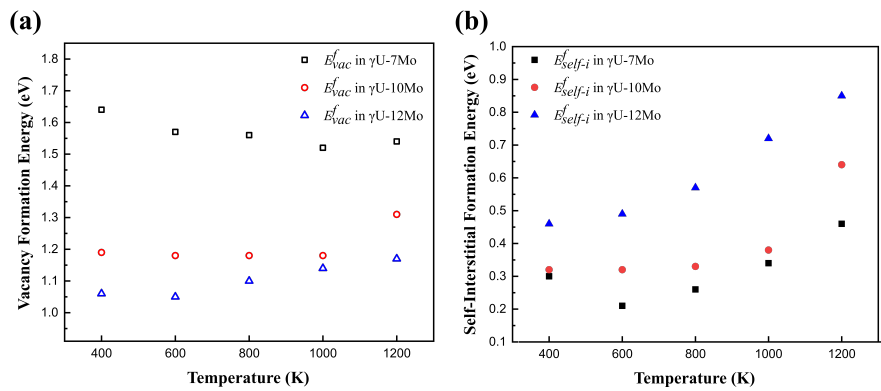


Figure 4: (a) Vacancy formation energy and (b) self-interstitial formation energy in γ U-xMo as a function of temperature. The standard errors for vacancy and self-interstitial formation energies were less than 0.3 eV at each temperature and composition.

257 3.4. Self-diffusion and interdiffusion coefficients in γ U-Mo

258 Fig. 5(a)-(c) represent the mean-square displacements of U and Mo (per atom) in
 259 γ U-xMo containing a self-interstitial with respect to time. The mean-square displace-
 260 ments of U and Mo below 800 K are not represented due to their insignificant diffusion

261 within these time scales. The results of the mean-square displacements of U and Mo
262 in γ U-xMo containing a vacancy are also not shown since they were negligible within
263 the temperature ranges of 400 K to 1200 K. In γ U-7Mo, the mean-square displacement
264 of Mo was consistently greater than that of U in the temperature range between 800
265 K and 1200 K. The mean-square displacement of Mo was also higher than that of U
266 in γ U-10Mo at all simulation temperatures, but the magnitude of their differences de-
267 creased in comparison to γ U-7Mo. In γ U-12Mo, the mean-square displacement of U
268 was slightly greater than that of Mo at equivalent temperatures at the end of the 100 ns
269 simulation time. However, in γ U-12Mo at 1000 K and 1200 K at the beginning of the
270 simulation, the diffusion of U was slower than that of Mo.

271 Utilizing the point defect formation energies from *Section 3.3*, the equilibrium de-
272 fect concentrations were calculated, which allowed for the determination of self-diffusion
273 coefficients using Eq. (9) and (10). The equilibrium concentrations of vacancy and
274 self-interstitial were found to be 2.4×10^{-5} and 2.5×10^{-3} in γ U-12Mo at 1200 K,
275 respectively, as an example. Fig. 5(d) and Table 2 represent the self-diffusion coef-
276 ficients as a function of temperature in γ U-xMo. To highlight the differences in the
277 self-diffusion coefficients of U and Mo atoms, the tabular form is also provided (Table
278 2). The self-diffusion coefficients of both U and Mo atoms decreased as the concen-
279 tration of Mo increased, which are in qualitative agreement with previous experimental
280 investigations [59]. In addition, the self-diffusion coefficients of U atoms were higher
281 than the self-diffusion coefficients of Mo atoms at the investigated compositions and
282 temperatures. The ratios of the self-diffusion coefficient of Mo atoms to that of U atoms
283 were 3–4 in the temperature range of 800 K to 1200 K in γ U-xMo, which is also qual-
284 itatively agreed with the experimental results [59]. The experimental results indicated
285 that intrinsic diffusion coefficients of U atoms were greater than that of Mo atoms by a
286 factor of 5–7 at the annealing temperatures of 1073 K, 1173 K, and 1273 K [59]. Sim-
287 ilarly, a previous MD study in γ U-9Mo showed that the self-diffusion coefficients of
288 U atoms were greater than those of Mo atoms by a factor of 4–12 in the temperature
289 range 800 K to 1400 K using the U-Mo-Xe potential [26].

290 The interdiffusion coefficients in γ U-xMo are represented with respect to tempera-
291 ture in Fig. 6 along with the experimental results in the equivalent composition ranges.

292 The interdiffusion coefficients in the U-Mo alloys were calculated using the fitted Mo
 293 concentration profiles from a U-Mo diffusion couple via the Boltzmann-Matano anal-
 294 ysis [60]. The interdiffusion coefficients, calculated from both the experiment and
 295 this work, decreased with increasing Mo concentration. The pre-exponential factors
 296 ($D_{0,inter-D}$) and activation energies ($Q_{inter-D}$), calculated from the Arrhenius plot of the
 297 interdiffusion coefficients, were compared to the experimental results, as shown in Ta-
 298 ble 3 and Table 4, respectively. The interdiffusion activation energies increased with
 299 Mo concentration and were in qualitative agreement with experimental observations
 300 [59]. However, the interdiffusion activation energies in the experimental results were
 301 1.8–2.4 times greater than the current work [59]. The discrepancy between experimen-
 302 tal results and computational results could be due to a number of factors, including the
 303 interatomic potential and the comparatatively short time scale of MD simulations.

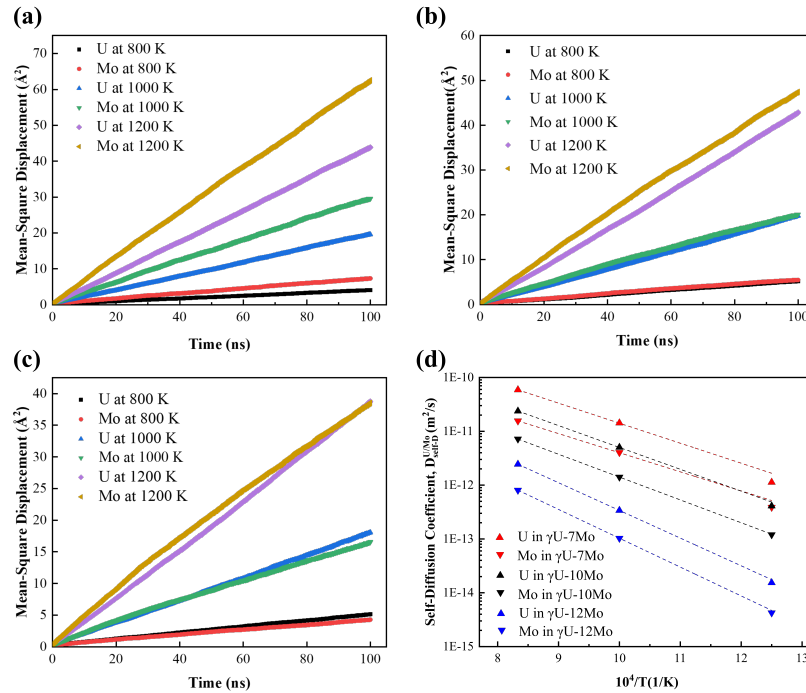


Figure 5: The mean-square displacements of U and Mo atoms with respect to time in (a) $\gamma\text{U}-7\text{Mo}$, (b) $\gamma\text{U}-10\text{Mo}$, (c) $\gamma\text{U}-12\text{Mo}$ containing a self-interstitial. Note the differences in y-scales. (d) The self-diffusion coefficient of U and Mo atoms in $\gamma\text{U}-\text{Mo}$ with respect to temperature and composition. The self-diffusion coefficients in each composition were fitted to the Arrhenius equation.

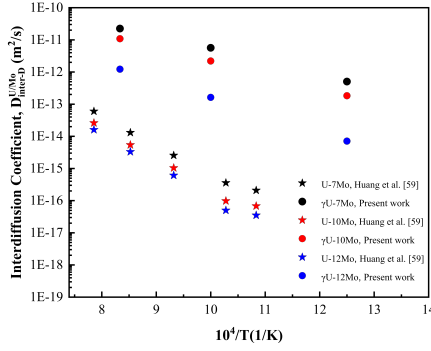


Figure 6: The interdiffusion coefficients in γ U-xMo with respect to temperature and composition along with the experimental results [59].

Table 2: Self-diffusion coefficients ($D_{self-D}^{U/Mo}$) of U and Mo atoms in γ U-xMo.

Composition	Temperature (K)	D_{self-D}^U (m ² /s)	D_{self-D}^{Mo} (m ² /s)	$D_{self-D}^U/D_{self-D}^{Mo}$
γ U-7Mo	800	1.13×10^{-12}	3.88×10^{-13}	2.91
	1000	1.43×10^{-11}	4.04×10^{-12}	3.53
	1200	5.89×10^{-11}	1.56×10^{-11}	3.78
γ U-10Mo	800	4.13×10^{-13}	1.20×10^{-13}	3.44
	1000	5.03×10^{-12}	1.41×10^{-12}	3.57
	1200	2.38×10^{-11}	7.18×10^{-12}	3.31
γ U-12Mo	800	1.54×10^{-14}	4.24×10^{-15}	3.63
	1000	3.39×10^{-13}	1.03×10^{-13}	3.29
	1200	2.44×10^{-12}	8.05×10^{-13}	3.05

Table 3: Comparison of pre-exponential factors (D_0) in γ U- x Mo. Units are m^2/s .

Composition	$D_{0,\text{self-}D}^U$ ¹	$D_{0,\text{self-}D}^{\text{Mo}}$ ²	$D_{0,\text{inter-}D}$ ³	$D_{0,\text{inter-}D}^{\text{exp}}$ ⁴
γ U-7Mo	1.78×10^{-7}	2.74×10^{-8}	4.83×10^{-8}	1.32×10^{-6}
γ U-10Mo	8.40×10^{-8}	2.59×10^{-8}	3.85×10^{-8}	7.70×10^{-7}
γ U-12Mo	6.34×10^{-8}	2.98×10^{-8}	3.72×10^{-8}	5.70×10^{-7}

^{1,2} D_0 of U and Mo self-diffusion in γ U- x Mo, respectively.

³ D_0 of interdiffusion in γ U- x Mo from the current work.

⁴ D_0 of interdiffusion in γ U- x Mo from experiments [59].

Table 4: Comparison of activation energies (Q) in γ U- x Mo. Units are eV.

Composition	$Q_{\text{self-}D}^U$ ¹	$Q_{\text{self-}D}^{\text{Mo}}$ ²	$Q_{\text{inter-}D}$ ³	$Q_{\text{inter-}D}^{\text{exp}}$ ⁴
γ U-7Mo	0.82	0.77	0.79	1.86
γ U-10Mo	0.84	0.85	0.84	1.89
γ U-12Mo	1.05	1.09	1.07	1.91

^{1,2} Self-diffusion activation energy of U and Mo, respectively.

³ Interdiffusion activation energy in γ U- x Mo.

⁴ Interdiffusion activation energy in γ U- x Mo from experiments [59].

304 4. Discussion

305 The vacancy formation energy in γ U- x Mo decreased with increasing Mo concentration.
 306 The vacancy formation energies in pure Mo, obtained via PAS and first-principles
 307 calculations, ranged from 1.6 eV to 3.6 eV, and tended to be greater than that of γ U
 308 [61, 62, 63, 64, 65, 66]. This seems to indicate that the bond energy between U and
 309 Mo atoms is lower than the bond energy between U and U atoms. Thus, it might be
 310 easier to create a vacancy if more Mo neighbors exist in the alloy. The mixing enthalpy
 311 calculated both experimentally and computationally support this proposed hypothesis
 312 [67, 68]. A mixing enthalpy in γ U-Mo was found to be positive over the whole com-

³¹³ position range at 1000 K using MD simulations [67]. The positive mixing enthalpy in
³¹⁴ γ U-Mo was also experimentally observed when the concentration of Mo was greater
³¹⁵ than 7 wt.% at 1100 K [68]. The mixing enthalpy is positive when the internal energy
³¹⁶ following mixing is greater than the internal energy prior to the mixing. This indicates
³¹⁷ that the U-Mo bond is weaker than the U-U bond, and thus the U-Mo bond is not favor-
³¹⁸ able. Vacancy formation energies in alloys are dependent on the types of atoms present
³¹⁹ and their concentrations surrounding a vacancy [69, 70, 71, 72, 73].

³²⁰ The self-interstitial formation energy increased as the Mo concentration increased at
³²¹ the investigated temperatures since the self-interstitial formation energy in Mo [56, 74]
³²² is greater than that of γ U, irrespective of the self-interstitial atom configuration. Thus,
³²³ the creation of a self-interstitial requires more energy as the concentration of Mo is in-
³²⁴ creased.

³²⁵ Since the vacancy formation energy was found to be greater than the self-interstitial
³²⁶ formation energy in γ U and γ U-xMo at temperatures from 400 K to 1200 K, the concen-
³²⁷ tration of self-interstitials will be higher than the vacancy concentration at equilibrium.
³²⁸ This further confirms that self-diffusion is dominated by self-interstitials in both γ U
³²⁹ and γ U-xMo, as previously suggested [26]. The self-interstitial dominated diffusion
³³⁰ was also supported by the mean-square displacement calculations in γ U-xMo contain-
³³¹ ing a self-interstitial atom, which were higher than those containing a vacancy.

³³² The self-diffusion and interdiffusion coefficients in γ U-xMo decreased with in-
³³³ creasing Mo concentration. Since the self-interstitial formation energies were lower
³³⁴ than the vacancy formation energies in γ U-xMo at the investigated temperatures, the
³³⁵ self-diffusion coefficients were dominated by the self-interstitial terms in Eq. (9) and
³³⁶ (10). An exponentially decreased equilibrium concentration of self-interstitials, which
³³⁷ is primarily attributed to an increase in self-interstitial formation energies, resulted in
³³⁸ a decrease in self-diffusion coefficients with increasing Mo concentration. The va-
³³⁹ cancy terms in Eq. (9) and (10) were found to be negligible due to the higher vacancy
³⁴⁰ formation energies, which reduced the concentration of vacancies exponentially. The
³⁴¹ interdiffusion coefficients in γ U-xMo, calculated using the self-diffusion coefficients
³⁴² in this work, compare well to previous observations [59].

³⁴³ **5. Conclusions**

³⁴⁴ In the present work, vacancy and self-interstitial formation energies in γ U and γ U-
³⁴⁵ xMo as well as the self-diffusion/interdiffusion coefficients in γ U-xMo were calculated
³⁴⁶ with MD simulations using the EAM U-Mo-Xe potential [37]. In γ U, the vacancy
³⁴⁷ formation energy increased with increasing temperature, ranging between 1.74 eV and
³⁴⁸ 2.43 eV. However, there was little temperature dependency on the self-interstitial for-
³⁴⁹ mation energy. The lower and upper limits of the self-interstitial formation energy were
³⁵⁰ 0.90 eV and 1.08 eV, respectively. In γ U-xMo, the vacancy formation energy decreased
³⁵¹ with increasing Mo content, while the self-interstitial formation energy increased with
³⁵² increasing Mo content in the temperature range between 400 K and 1200 K. The self-
³⁵³ interstitial formation energy was lower than the vacancy formation energy in both γ U
³⁵⁴ and γ U-xMo at the investigated temperature range, which agrees with the previous
³⁵⁵ studies that utilized first principles calculations and MD simulations with various in-
³⁵⁶ teratomic potentials [21, 26, 27, 28, 37, 49, 50]. These results indicate that diffusion
³⁵⁷ occurs primarily via self-interstitials in γ U and γ U-xMo.

³⁵⁸ The calculated formation energies of vacancies and self-interstitials were utilized to
³⁵⁹ determine the self-diffusion/interdiffusion coefficients in γ U-xMo in the investigated
³⁶⁰ temperature range. As the Mo concentration increased, the self-diffusion/interdiffusion
³⁶¹ coefficients decreased and their diffusion activation energies increased, which are qual-
³⁶² itatively consistent with the previous experimental results [59]. The point defect for-
³⁶³ mation energies, self-diffusion coefficients, and interdiffusion coefficients, obtained
³⁶⁴ from the current MD simulations, can be used as input parameters in **microscale and**
³⁶⁵ **mesoscale** nuclear fuel models, such as kinetic Monte Carlo, phase-field, and cluster
³⁶⁶ dynamics. These newly calculated parameters will help to more accurately simulate the
³⁶⁷ microstructural evolution under irradiation, including fission gas swelling and recrys-
³⁶⁸ tallization.

³⁶⁹ **6. CRediT author statement**

³⁷⁰ **Gyuchul Park:** Conceptualization, Formal analysis, Investigation, Methodology,
³⁷¹ Visualization, Writing-original draft. **Benjamin Beeler:** Conceptualization, Funding

³⁷² acquisition, Methodology, Project administration, Resources, Supervision, Writing-
³⁷³ review and editing. **Maria A. Okuniewski:** Conceptualization, Funding acquisition,
³⁷⁴ Methodology, Project administration, Resources, Supervision, Writing-review and edit-
³⁷⁵ ing.

³⁷⁶ **7. Acknowledgements**

³⁷⁷ This work was supported by the U.S. Department of Energy, Office of Material
³⁷⁸ Management and Minimization, National Nuclear Security Administration, under DOE-
³⁷⁹ NE Idaho Operations Office Contract DE-AC07-05ID14517. This research made use
³⁸⁰ of the High Performance Computing Center at Idaho National Laboratory, which is
³⁸¹ supported by the Office of Nuclear Energy of the U.S. Department of Energy and the
³⁸² Nuclear Science User Facilities.

³⁸³ **References**

- ³⁸⁴ [1] J. Kittel, B. Frost, J. Mustelier, K. Bagley, G. Crittenden, J. Van Dievoet, History
³⁸⁵ of fast reactor fuel development, Journal of Nuclear Materials 204 (1993) 1–13.
- ³⁸⁶ [2] J. Snelgrove, G. Hofman, M. Meyer, C. Trybus, T. Wienczek, Development of
³⁸⁷ very-high-density low-enriched-uranium fuels, Nuclear Engineering and Design
³⁸⁸ 178 (1997) 119–126.
- ³⁸⁹ [3] R. Prabhakaran, U-Mo Monolithic Fuel for Nuclear Research and Test Reactors,
³⁹⁰ JOM 69 (2017) 2529–2531.
- ³⁹¹ [4] J. Rest, Y. S. Kim, G. L. Hofman, M. K. Meyer, S. L. Hayes, U-Mo fuels
³⁹² handbook. Version 1.0 (No. ANL-09/31), Technical Report, Argonne National
³⁹³ Lab.(ANL), Argonne, IL (United States), 2006.
- ³⁹⁴ [5] G. Lander, E. Fisher, S. Bader, The solid-state properties of uranium a historical
³⁹⁵ perspective and review, Advances in Physics 43 (1994) 1–111.

- 396 [6] M. Meyer, J. Gan, J. Jue, D. Keiser, E. Perez, A. Robinson, D. Wachs, N. Wool-
397 stenhueme, G. Hofman, Y. Kim, Irradiation performance of U-Mo monolithic
398 fuel, Nuclear Engineering and Technology 46 (2014) 169–182.
- 399 [7] S. Neogy, M. Saify, S. Jha, D. Srivastava, M. Hussain, G. Dey, R. Singh, Mi-
400 crostructural study of gamma phase stability in U-9 wt.%Mo alloy, Journal of
401 Nuclear Materials 422 (2012) 77–85.
- 402 [8] R. Hills, B. Howlett, B. Butcher, Further studies on the decomposition of the γ
403 phase in uranium-low molybdenum alloys, Journal of the Less Common Metals
404 5 (1963) 369–373.
- 405 [9] K. H. Kim, D. B. Lee, C. K. Kim, G. E. Hofman, K. W. Paik, Characterization of
406 U-2 wt% Mo and U-10 wt% Mo alloy powders prepared by centrifugal atomiza-
407 tion, Journal of Nuclear Materials 245 (1997) 179–184.
- 408 [10] V. Sinha, P. Hegde, G. Prasad, G. Dey, H. Kamath, Effect of molybdenum addi-
409 tion on metastability of cubic γ -uranium, Journal of Alloys and Compounds 491
410 (2010) 753–760.
- 411 [11] V. Sinha, P. Hegde, G. Prasad, G. Dey, H. Kamath, Phase transformation of
412 metastable cubic γ -phase in U–Mo alloys, Journal of Alloys and Compounds 506
413 (2010) 253–262.
- 414 [12] L. Mansur, Effects of point defect trapping and solute segregation on irradiation-
415 induced swelling and creep, Technical Report, Oak Ridge National Lab., TN
416 (USA), 1978.
- 417 [13] L. Mansur, T. Reiley, Irradiation creep by dislocation glide enabled by preferred
418 absorption of point defects—theory and experiment, Journal of Nuclear Materials
419 90 (1980) 60–67.
- 420 [14] C. Pokor, Y. Brechet, P. Dubuisson, J.-P. Massoud, X. Averty, Irradiation damage
421 in 304 and 316 stainless steels: experimental investigation and modeling. Part II:
422 Irradiation induced hardening, Journal of Nuclear Materials 326 (2004) 30–37.

- 423 [15] N. Peterson, Diffusion in the anomalous bcc metals, *Comments on Solid State*
424 *Physics* 8 (1978) 93–106.
- 425 [16] H. Matter, J. Winter, W. Triftshäuser, Investigation of vacancy formation and
426 phase transformations in uranium by positron annihilation, *Journal of Nuclear*
427 *Materials* 88 (1980) 273–278.
- 428 [17] G. Kögel, P. Sperr, W. Triftshäuser, S. Rothman, Positron lifetime and doppler-
429 broadening studies of vacancy formation and phase transformation in uranium,
430 *Journal of Nuclear Materials* 131 (1985) 148–157.
- 431 [18] K. Lund, K. Lynn, M. Weber, M. Okuniewski, Vacancy formation enthalpy in
432 polycrystalline depleted uranium, *Journal of Physics: Conference Series* 443
433 (2013) 012021.
- 434 [19] K. Lund, K. Lynn, M. Weber, C. Macchi, A. Somoza, A. Juan, M. Okuniewski,
435 Impurity migration and effects on vacancy formation enthalpy in polycrystalline
436 depleted uranium, *Journal of Nuclear Materials* 466 (2015) 343–350.
- 437 [20] S. Xiang, H. Huang, L. Hsiung, Quantum mechanical calculations of uranium
438 phases and niobium defects in γ -uranium, *Journal of Nuclear Materials* 375 (2008)
439 113–119.
- 440 [21] B. Beeler, B. Good, S. Rashkeev, C. Deo, M. Baskes, M. Okuniewski, First prin-
441 ciples calculations for defects in U, *Journal of Physics: Condensed Matter* 22
442 (2010) 505703.
- 443 [22] J. P. Perdew, J. A. Chevary, S. H. Vosko, K. A. Jackson, M. R. Pederson, D. J.
444 Singh, C. Fiolhais, Atoms, molecules, solids, and surfaces: Applications of the
445 generalized gradient approximation for exchange and correlation, *Physical Re-
446 view B* 46 (1992) 6671.
- 447 [23] J. P. Perdew, K. Burke, M. Ernzerhof, Generalized gradient approximation made
448 simple, *Physical Review Letters* 77 (1996) 3865.

- 449 [24] S. Rothman, L. Lloyd, R. Weil, A. Harkness, Self-diffusion in gamma uranium,
450 Technical Report, Argonne National Lab., Lemont, Ill., 1959.
- 451 [25] S. Rothman, The diffusion of gold in gamma uranium, *Journal of Nuclear Mate-*
452 *rials* 3 (1961) 77–80.
- 453 [26] D. Smirnova, A. Y. Kuksin, S. Starikov, V. Stegailov, Atomistic modeling of the
454 self-diffusion in γ -U and γ -U-Mo, *The Physics of Metals and Metallography* 116
455 (2015) 445–455.
- 456 [27] D. Smirnova, A. Y. Kuksin, S. Starikov, Investigation of point defects diffusion in
457 bcc uranium and U–Mo alloys, *Journal of Nuclear Materials* 458 (2015) 304–311.
- 458 [28] B. Beeler, S. Hu, Y. Zhang, Y. Gao, A improved equation of state for Xe gas
459 bubbles in γ U-Mo fuels, *Journal of Nuclear Materials* 530 (2020) 151961.
- 460 [29] S. Plimpton, Fast parallel algorithms for short-range molecular dynamics, *Journal*
461 *of Computational Physics* 117 (1995) 1–19.
- 462 [30] M. S. Daw, M. I. Baskes, Embedded-atom method: Derivation and application
463 to impurities, surfaces, and other defects in metals, *Physical Review B* 29 (1984)
464 6443.
- 465 [31] S. Foiles, Calculation of the surface segregation of Ni-Cu alloys with the use of
466 the embedded-atom method, *Physical Review B* 32 (1985) 7685.
- 467 [32] S. Foiles, M. Baskes, M. S. Daw, Embedded-atom-method functions for the fcc
468 metals Cu, Ag, Au, Ni, Pd, Pt, and their alloys, *Physical Review B* 33 (1986)
469 7983.
- 470 [33] D. Oh, R. Johnson, Simple embedded atom method model for fcc and hcp metals,
471 *Journal of Materials Research* 3 (1988) 471–478.
- 472 [34] M. S. Daw, S. M. Foiles, M. I. Baskes, The embedded-atom method: a review of
473 theory and applications, *Materials Science Reports* 9 (1993) 251–310.

- 474 [35] P. Williams, Y. Mishin, J. Hamilton, An embedded-atom potential for the Cu–
475 Ag system, Modelling and Simulation in Materials Science and Engineering 14
476 (2006) 817.
- 477 [36] M. S. Daw, M. I. Baskes, Semiempirical, quantum mechanical calculation of
478 hydrogen embrittlement in metals, Physical Review Letters 50 (1983) 1285.
- 479 [37] D. Smirnova, A. Y. Kuksin, S. Starikov, V. Stegailov, Z. Insepov, J. Rest, A. Ya-
480 cout, A ternary EAM interatomic potential for U–Mo alloys with xenon, Mod-
481elling and Simulation in Materials Science and Engineering 21 (2013) 035011.
- 482 [38] B. Beeler, B. Good, S. Rashkeev, C. Deo, M. Baskes, M. Okuniewski, First-
483 principles calculations of the stability and incorporation of helium, xenon and
484 krypton in uranium, Journal of Nuclear Materials 425 (2012) 2–7.
- 485 [39] B. Beeler, C. Deo, M. Baskes, M. Okuniewski, Atomistic investigations of intrin-
486 sic and extrinsic point defects in bcc uranium, ASTM International 25 (2013).
- 487 [40] X. Hong-Xing, T. Rui, T. Xiao-Feng, L. Chong-Sheng, Molecular dynamics sim-
488 ulation of Xe behavior in U–Mo alloys fuel, Chinese Physics Letters 31 (2014)
489 047101.
- 490 [41] Y. Miao, B. Beeler, C. Deo, M. I. Baskes, M. A. Okuniewski, J. F. Stubbins, Defect
491 structures induced by high-energy displacement cascades in γ uranium, Journal
492 of Nuclear Materials 456 (2015) 1–6.
- 493 [42] S. Hu, W. Setyawan, V. V. Joshi, C. A. Lavender, Atomistic simulations of ther-
494 modynamic properties of Xe gas bubbles in U10Mo fuels, Journal of Nuclear
495 Materials 490 (2017) 49–58.
- 496 [43] N. Grønbech-Jensen, O. Farago, A simple and effective Verlet-type algorithm for
497 simulating Langevin dynamics, Molecular Physics 111 (2013) 983–991.
- 498 [44] N. Grønbech-Jensen, N. R. Hayre, O. Farago, Application of the G-JF discrete-
499 time thermostat for fast and accurate molecular simulations, Computer Physics
500 Communications 185 (2014) 524–527.

- 501 [45] J. D. Honeycutt, H. C. Andersen, Molecular dynamics study of melting and freez-
502 ing of small Lennard-Jones clusters, *Journal of Physical Chemistry* 91 (1987)
503 4950–4963.
- 504 [46] A. Stukowski, Structure identification methods for atomistic simulations of crys-
505 talline materials, *Modelling and Simulation in Materials Science and Engineering*
506 20 (2012) 045021.
- 507 [47] A. Stukowski, Visualization and analysis of atomistic simulation data with
508 OVITO—the Open Visualization Tool, *Modelling and Simulation in Materials*
509 *Science and Engineering* 18 (2009) 015012.
- 510 [48] L. S. Darken, Diffusion, mobility and their interrelation through free energy in
511 binary metallic systems, *Trans. Aime* 175 (1948) 184–201.
- 512 [49] B. Beeler, C. Deo, M. Baskes, M. Okuniewski, Atomistic properties of γ uranium,
513 *Journal of Physics: Condensed Matter* 24 (2012) 075401.
- 514 [50] D. Smirnova, S. Starikov, V. Stegailov, Interatomic potential for uranium in a
515 wide range of pressures and temperatures, *Journal of Physics: Condensed Matter*
516 24 (2011) 015702.
- 517 [51] M. I. Mendelev, B. S. Bokstein, Molecular dynamics study of vacancy migration
518 in Al, *Materials Letters* 61 (2007) 2911–2914.
- 519 [52] M. I. Mendelev, Y. Mishin, Molecular dynamics study of self-diffusion in bcc Fe,
520 *Physical Review B* 80 (2009) 144111.
- 521 [53] M. I. Mendelev, B. S. Bokstein, Molecular dynamics study of self-diffusion in Zr,
522 *Philosophical Magazine* 90 (2010) 637–654.
- 523 [54] R. Johnson, Many-body effects on calculated defect properties in hcp metals,
524 *Philosophical Magazine A* 63 (1991) 865–872.
- 525 [55] Y. Mishin, M. R. Sørensen, A. F. Voter, Calculation of point-defect entropy in
526 metals, *Philosophical Magazine A* 81 (2001) 2591–2612.

- 527 [56] D. Nguyen-Manh, A. Horsfield, S. Dudarev, Self-interstitial atom defects in bcc
528 transition metals: Group-specific trends, *Physical Review B* 73 (2006) 020101.
- 529 [57] P. A. Olsson, Semi-empirical atomistic study of point defect properties in bcc
530 transition metals, *Computational Materials Science* 47 (2009) 135–145.
- 531 [58] B.-J. Lee, J.-H. Shim, M. Baskes, Semiempirical atomic potentials for the fcc
532 metals Cu, Ag, Au, Ni, Pd, Pt, Al, and Pb based on first and second nearest-
533 neighbor modified embedded atom method, *Physical Review B* 68 (2003) 144112.
- 534 [59] K. Huang, D. D. Keiser, Y. Sohn, Interdiffusion, intrinsic diffusion, atomic mobil-
535 ity, and vacancy wind effect in γ (bcc) uranium-molybdenum alloy, *Metallurgical*
536 and *Materials Transactions A* 44 (2013) 738–746.
- 537 [60] H. Mehrer, Diffusion in solids: fundamentals, methods, materials, diffusion-
538 controlled processes, volume 155, Springer Science & Business Media, 2007.
- 539 [61] H.-E. Schaefer, Investigation of thermal equilibrium vacancies in metals by
540 positron annihilation, *Physica Status Solidi (a)* 102 (1987) 47–65.
- 541 [62] H. Ullmaier, P. Ehrhart, P. Jung, H. Schultz, Atomic defects in metals, volume 3,
542 Springer, 1991.
- 543 [63] T. Korhonen, M. J. Puska, R. M. Nieminen, Vacancy-formation energies for fcc
544 and bcc transition metals, *Physical Review B* 51 (1995) 9526.
- 545 [64] T. R. Mattsson, A. E. Mattsson, Calculating the vacancy formation energy in
546 metals: Pt, Pd, and Mo, *Physical Review B* 66 (2002) 214110.
- 547 [65] T. R. Mattsson, N. Sandberg, R. Armiento, A. E. Mattsson, Quantifying the
548 anomalous self-diffusion in molybdenum with first-principles simulations, *Phys-*
549 *ical Review B* 80 (2009) 224104.
- 550 [66] B. Medasani, M. Haranczyk, A. Canning, M. Asta, Vacancy formation energies
551 in metals: A comparison of MetaGGA with LDA and GGA exchange–correlation
552 functionals, *Computational Materials Science* 101 (2015) 96–107.

- 553 [67] S. Starikov, L. Kolotova, A. Y. Kuksin, D. Smirnova, V. Tseplyaev, Atomistic
554 simulation of cubic and tetragonal phases of U-Mo alloy: Structure and thermo-
555 dynamic properties, Journal of Nuclear Materials 499 (2018) 451–463.
- 556 [68] Y. V. Vamberskiy, A. Udovskiy, O. Ivanov, Experimental determination and cal-
557 culation of excess thermodynamic functions of molybdenum solid solutions in
558 gamma-uranium, Journal of Nuclear Materials 46 (1973) 192–206.
- 559 [69] J. M. Sampedro, E. Del Rio, M. J. Caturla, M. Victoria, J. M. Perlado, Defect en-
560 ergetics in Fe–Cr alloys from empirical interatomic potentials, Journal of Nuclear
561 Materials 417 (2011) 1050–1053.
- 562 [70] E. Del Rio, J. M. Sampedro, H. Dogo, M. J. Caturla, M. Caro, A. Caro, J. M.
563 Perlado, Formation energy of vacancies in FeCr alloys: Dependence on Cr con-
564 centration, Journal of Nuclear Materials 408 (2011) 18–24.
- 565 [71] S. Zhao, G. M. Stocks, Y. Zhang, Defect energetics of concentrated solid-
566 solution alloys from ab initio calculations: $\text{Ni}_{0.5}\text{Co}_{0.5}$, $\text{Ni}_{0.5}\text{Fe}_{0.5}$, $\text{Ni}_{0.8}\text{Fe}_{0.2}$ and
567 $\text{Ni}_{0.8}\text{Cr}_{0.2}$, Physical Chemistry Chemical Physics 18 (2016) 24043–24056.
- 568 [72] W. Chen, X. Ding, Y. Feng, X. Liu, K. Liu, Z. Lu, D. Li, Y. Li, C. Liu, X.-Q. Chen,
569 Vacancy formation enthalpies of high-entropy FeCoCrNi alloy via first-principles
570 calculations and possible implications to its superior radiation tolerance, Journal
571 of Materials Science & Technology 34 (2018) 355–364.
- 572 [73] A. Esfandiarpour, M. Nasrabadi, Vacancy formation energy in CuNiCo equimolar
573 alloy and CuNiCoFe high entropy alloy: ab initio based study, Calphad 66 (2019)
574 101634.
- 575 [74] S. Han, L. A. Zepeda-Ruiz, G. J. Ackland, R. Car, D. J. Srolovitz, Self-interstitials
576 in V and Mo, Physical Review B 66 (2002) 220101.